Journal of the European Ceramic Society 20 (2000) 1959–1974

Oxidation behaviour of ceramic fibres from the Si–C–N–O system and related sub-systems

Georges Chollon

Laboratoire des Composites Thermostructuraux, UMR 5801, CNRS-SNECMA-CEA-UB1, Université de Bordeaux-1, 3 allée de La Boétie, 33600 Pessac France

Received 16 December 1999; accepted 21 March 2000

Abstract

The oxidation of Si–C–N–O fibres has been investigated. The oxidation rates and the activation energies for the Si–C–O system are similar to those for crystalline SiC. The oxygen and the free carbon concentrations in the ceramics have a limited influence on the oxidation behaviour. As long as the formed silica scale is protective, oxidation kinetics are essentially controlled by the diffusion of oxygen through SiO_2. The parabolic rates in the Si–C–N–O and Si–N–O systems are lower and their activation energies higher than those for SiC. Their values strongly depend on the ratios of C and N bonds to Si and continuously vary from those for SiC ($E_a = 110 - 140$kJ mol^{-1}) to Si_3N_4 ($E_a = 330-490$ kJ mol^{-1}). The oxidation mechanism might be related to a complex diffusion/reaction regime via the formation of an intermediate silicon-oxynitride (like for Si_3N_4) or silicon-oxycarbonitride layer. The oxidation behaviour of such complex systems is not significantly influenced by the oxygen nor the free carbon contents. It might be governed by the C/Si and N/Si ratios, limiting the nitrogen concentration gradient of the silicon-oxy(carbo)nitride sub-layer and therefore affecting the diffusion/reaction rates.

Keywords: Fibres; Oxidation; SiC; Si_3N_4; Si–C–N–O

1. Introduction

Crystalline silicon-based ceramics such as silicon carbide (SiC) or silicon nitride (Si_3N_4) are high temperature structural materials of prime interest because of their excellent properties in thermal shock resistance, corrosion resistance, creep resistance and high strength and stiffness retention at elevated temperature.[1] Silicon-oxynitride (Si_2N_2O) is also remarkable for its high strength, low thermal expansion, abrasion resistance and its excellent chemical stability in acid, molten non ferrous metals and air at high temperature.[2] Ceramics belonging to the Si–C–N–O system and the various related sub-systems (e.g. Si–C–N, Si–C–O, Si–N–O and Si–C) are therefore attractive candidates for high temperature structural applications in corrosive media. Polymeric precursor pyrolysis and chemical vapour deposition (CVD) processing techniques are suitable to control the composition and the properties of such complex systems. They have been successively used to synthesise small diameter ceramic fibres and whiskers of various compositions, for the reinforcement of metal and ceramic matrix composites (MMC and CMC).[3–21] Such complex quaternary and ternary systems generally give rise to combinations of covalent structures, either amorphous or nanocrystalline.[3–26] One of the most important issues regarding the application of ceramic fibres as reinforcement for high temperature structures, is their thermal stability. Decomposition and/or crystallisation of the silicon-oxycarbonitride metastable phases may therefore be expected at high temperature (beyond the processing temperature), resulting in a degradation of the mechanical properties.[14–17,21,26–35] Another key thermal characteristic of ceramics from these complex systems is their oxidation resistance. The high oxidation resistance of Si-based ceramics is attributed to the growth of a protective silica film in the passive regime. The oxidation of pure silicon, crystalline SiC (monocrystals and polycrystalline CVD layers) and Si_3N_4 (polycrystalline CVD films) has been extensively studied. The growth of the silica layer thickness generally exhibits a parabolic time dependence but with radically different kinetics and thermal dependence. The parabolic constants of oxidation for Si_3N_4 are generally lower than those for Si and SiC at low temperature

E-mail address: chollon@lcts.u-bordeaux.fr (G.Chollon).

0955-2219/00/$ - see front matter
PII: S0955-2219(00)00101-1

($T < 1400°C$) and have a much higher thermal activation.[36–62] The oxidation kinetics of ceramics from the Si–C–N–O system and the related ternary subsystems (Si–C–N, Si–C–O and Si–N–O) have seldom been reported. Few studies have been dedicated to the oxidation of Si–C–N–O, Si–C–O and Si–C fibres,[63–70] however, their respective oxidation kinetics have not been discussed in details so far. For instance, the influence of the oxygen concentration, the carbon to nitrogen ratio in the ceramics and the presence of free carbon, which is commonly encountered in polymer derived ceramic fibres, have not been systematically investigated yet. The aim of this work was to achieve a comparative analysis of the oxidation of various fibres from the Si–C–N–O system. This analysis is based on the examination of the oxidation features of commercial or experimental fibres being investigated during the last few years, as well as crystalline compounds (SiC and Si_3N_4) reported in the literature.

2. Experimental

2.1. Description of the fibres

2.1.1. The Si–C–O fibre

Nicalon NL 200 fibre (from Nippon Carbon, Japan) is the most widely used SiC-based composites reinforcement for industrial applications. The fibre is fabricated through the spinning of a polycarbosilane (PCS), its curing, by simple oxidation in air (to make the filament infusible) and its final pyrolysis.[3] This fibre consists of nanometric SiC crystals (~2 nm), carbon clusters (~15 at.% of free carbon) and an amorphous silicon-oxycarbide phase, the oxygen (~13 at.%) being introduced during the curing step.[22–26] The Nicalon NL 200 has a limited thermal stability. The silicon-oxycarbide phase decomposes above 1100–1200°C into CO and SiO, leading to a strong decrease of strength.[26–31]

2.1.2. The Si–C–(O) fibre

This experimental low-oxygen SiC-based fibre was prepared from a commercial PCS (from Shin Etsu, Japan) modified to allow for melt spinning.[11] The PCS filaments were cured with an electron beam (EB) (dose of 1000 Mrad, with a rate of 300 Mrad h^{-1}) under an argon atmosphere. The irradiated filaments were subsequently pyrolysed under an argon flow up to 850°C with a heating rate of 50°C h^{-1}. The pyrolysis was then achieved under argon at the final treatment temperature $Tp = 1400°C$ for 0.25 h.

2.1.3. The Si–C fibre

This commercial Si-C fibre (Hi-Nicalon from Nippon Carbon, Japan) is also prepared from the spinning of PCS and subsequent electron beam curing process.[5–6] It has a very low oxygen content (< 0.5 at.%) and exhibits a remarkable thermal stability.[6,32–33]

2.1.4. The Si–Ti–C–(O) fibre

This fibre (Tyranno Lox-E from UBE, Japan) is prepared from a polytitanocarbosilane (PTCS) precursor synthesised by mixing polydimethylsilane (PDMS), polyborophenylsiloxane and a tetralkoxide titanate (Ti(OR)4).[4] Like the Hi-Nicalon fibre, the Tyranno Lox-E fibre is prepared by replacing the oxygen curing (currently used to process the standard Tyranno Lox-M fibre) by an electron beam curing process.[12]

2.1.5. The Si–C–N–O fibre

The precursor used was an original polycarbosilazane (PCSZ). It was prepared according to a procedure which has been described elsewhere.[14–15] The PCSZ was spun in the molten state and the filaments were cured under a mixture of pure oxygen ($P = 50$ kPa) and nitrogen ($P = 50$ kPa).[14] They were subsequently pyrolysed under a flow of pure argon up to 850°C with a heating rate of 50°C h^{-1}. The pyrolysis was then achieved under flowing nitrogen at the final treatment temperature $Tp = 1200°C$ for 0.25 h.

2.1.6. The Si–C–N–(O) fibre

This fibre was prepared from a polysilazane precursor (PSZ) (NCP200 from Chisso, Japan). The PSZ was spun and the green filaments were cured with an electron beam (EB) in the same conditions than the experimental low-oxygen PCS-derived fibres described below. The irradiated filaments were subsequently pyrolysed under an argon flow up to 850°C with a heating rate of 50°C h^{-1}. The pyrolysis was then achieved under argon or nitrogen at the final treatment temperature $Tp (1000 < Tp < 1600°C)$ for 0.25 h.[16]

2.1.7. The Si–N–O fibre

These fibres were prepared by a high temperature coreless CVD process developed at the Swiss Federal Laboratories for Materials Testing and Research (EMPA, Duebendorf, Switzerland). This process is described elsewhere.[21] The fibres were grown from silica powder deposited on a SiC substrate and heated at 1450°C for 16 h in an ammonia flow. The growth mechanism involves SiO(g) generated at SiO_2/SiC interface and ammonia-derived NH_x species resulting from the cracking of NH_3.

2.2. Characterisation techniques

Quantitative chemical analyses of the bulk of the fibres were performed on polished cross sections by electron probe microanalysis (EPMA) (CAMEBAX 75 from CAMECA, France) using wave length dispersion spectrometers (with a pentaerytritol crystal analyser for

Si-K_α and Ti-K_α and a PCII multilayer pseudo-crystal for C-K_α, N-K_α and O-K_α) and pure or stoichiometric standards (respectively SiC, Ti, Si_3N_4 and SiO_2). Hydrogen is not taken into account by EPMA.

The nanostructure of the fibres was investigated by high resolution transmission electron microscopy (TEM) (EM 400 from Philips). Crystalline phases analyses were also carried out by X-ray diffraction (XRD) (D5000 diffractometer from Siemens, Germany).

The oxidation kinetics of the fibres were studied by thermogravimetric analysis (TGA) (TAG 24 from Setaram, France). The experiments were performed on approximately 100 mg samples set in a pure alumina crucible and heated up to a maximum temperature T ranging from 800 to 1400°C. The heating rate was 1°C s^{-1} and the samples were maintained at an isothermal plateau at T for a time t ranging from 10 to 50 h under a pure oxygen flow ($P = 100$ kPa, $Q = 1\,l\,h^{-1}$). The silica layer resulting from the oxidation was also directly measured on fracture surface of the filament by means of scanning electron microscopy (SEM) analysis.

3. Results

3.1. Chemical and structural properties

The chemical composition of the various fibres is shown in Table 1 and the phase composition and the basic structural properties are summarised in Table 2.

3.1.1. The Si–C–O system and sub-systems

The oxygen content of the SiC-based electron beam-cured fibres is significantly lower than that of the oxygen-cured fibre (Si–C–O) (Table 1). All the fibres from the Si–C–O and Si–C systems contain significant amounts of free carbon. The EB-cured PCS and PTCS filaments [respectively Si–C-(O), Si–C and Si–Ti–C–(O) fibres] generally have a slightly higher free carbon content than the oxygen-cured PCS fibre (Si–C–O). The composition of the Si–C fibre is close (especially in terms of free carbon) to that of the Si–C–(O) fibre. The higher oxygen concentration of the latter fibre originates from the PCS precursor used which was pre-oxidised in its as-received state.[11] In addition to low amounts of titanium, the Si–Ti–C–(O) fibre shows a relatively high oxygen concentration. They both result from the composition of the starting PTCS precursor. The presence of hydrogen cannot be detected in the materials. However, significant amounts of hydrogen have been reported for the Si–C–O fibre.[24] It is also worthy of note that a neutron diffraction analysis qualitatively showed the presence of residual hydrogen in the Si–Ti–C–O fibre.[34]

Table 1
Chemical composition of the Si–C–N–O fibres

	Si(at.%)	Ti(at.%)	C(at.%)	N(at.%)	O(at.%)	C_1(at.%)
Si–C–O	39.0	0	45.0	0	16.0	14.0
Si–C–(O)	40.0	0	57.0	0	3.0	18.5
Si–C	41.0	0	58.0	0	1.0	17.5
Si–Ti–C–(O)	36.0	1.0	57.0	0	6.0	23.0
Si–C–N–O	36.0	0	28.0	14.0	22.0	13.5
Si–C–N–(O)	37.5	0	27.0	34.0	1.5	15.8
Si–N–O	40.9	0	0	45.1	14	0
SiC	50	0	50	0	0	0
Si_3N_4	42.9	0	0	57.1	0	0

All the N-free fibres contain a nanocrystallised β-SiC phase (Table 2). The mean apparent β-SiC grain size is about 2 nm for the Si–C–O fibre,[24] 4 nm for the Si–C–(O) fibre (currently ranging from 2 to 10 nm), 5 nm for the Si–C fibre (2 to 20 nm) and 2 nm for the Si–Ti–C–(O) (1–4 nm). The oxygen present in the fibres is under the form of an amorphous silicon(titanium) oxycarbide.[22–26,34] It is present in large amounts in the Si–C–O fibres whereas almost absent in the Si–C fibre. As suggested by the chemical analyses, they all exhibit free carbon organised as turbostratic stacks of graphene layers. The organisation of the carbon phase slightly differs in the different materials. It is present as BSUs (basic structural units, i.e. small stacks of $N = 2-3$ aromatic layers, $L_a = 1-2$ nm in extension) in the Si–C–O fibre[24] and slightly better organised in the Si–C–(O) ($N = 4-6$, $L_a = 3-5$ nm), Si–C ($N = 5-8$, $L_a = 2-3$ nm) and Si–Ti–C–(O) fibre ($N = 4-05$, $L_a = 1-3$ nm).

3.1.2. The Si–C–N–O system

The oxygen content of the EB-cured Si–C–N–(O) fibre is also much lower than that of the oxygen-cured fibre (Si–C–N–O). It is worthy of note that the two fibres were prepared from different precursors, the

Table 2
Microstructural features of the Si–C–N–O fibres

Si-C-O	Nano-crystallised SiC (~2 nm) + amorphous silicon oxcarbide + free carbon (basic structural units: BSU)
Si–C–(O)	Nano-crystallised SiC (4 nm) + traces of amorphous silicon oxcarbide + free carbon
Si–C	Nano-crystallised SiC (5 nm) + free carbon
Si–Ti–C–(O)	Nano-crystallised SiC (2 nm) + amorphous silicon/titanium oxycarbide + free carbon
Si–C–N–O	Amorphous silicon oxcarbonitride + free carbon
Si–C–N–(O)	Amorphous silicon (oxy)carbonitride + free carbon
Si–N–O	Amorphous silicon oxnitride

polysilazane precursor being richer in nitrogen than the polycarbosilazane. Consequently, the ceramic resulting from the polysilazane, has a much higher N/C atomic ratio. Both Si–C–N–O and Si–C–N–(O) fibres contain significant amounts of free carbon.

Both the Si–C–N–O and the Si–C–N–(O) fibres are amorphous on the basis of the X-ray and the electron diffraction. They consist of amorphous silicon oxycarbonitride phases of different compositions. TEM analyses also showed the presence of a free carbon phase in the Si–C–N–O fibre.[14] It was hardly evidenced under the form of BSUs, probably because of its poor structural organisation.

3.1.3. The Si–N–O system

With respect to the other fibres, the Si–N–O fibre is totally carbon free. Its chemical composition is comprised between those of Si_3N_4 and Si_2N_2O. It consists of an amorphous silicon oxynitride phase of chemical composition close to $SiN_{1.1}O_{0.3}$.[21]

All the fibres mentioned here belong to the Si–C–N–O system. Their chemical composition is defined by the atomic fractions c_{Si}, c_C, c_N and $c_O (0 \leqslant c_i \leqslant 1;\ \Sigma_i c_i = 1;\ i = \text{Si, C, N, O})$. It is represented by the point M on the composition quaternary diagram (Fig. 1). The fibres can be described as a combination of free carbon, with an atomic fraction $c_{Cf} (c_{Cf} \leqslant c_C)$ (except the carbon free Si–N–O fibre where $c_{cf} = c_c = 0$) and a silicon oxycarbonitride continuum, of atomic fractions $c'_i = c_i/(1 - c_{Cf})\ (i = \text{Si, N, O})$ and $c'_c = (c_C - c_{Cf})/(1 - c_{Cf})$, represented by the point M' in Fig. 1. Generally speaking, the silicon oxycarbonitride phase includes here either an amorphous silicon oxycarbonitride phase[25–26] (like for instance in the Si–C–N–O and Si–C–N–(O) fibres), a single amorphous silicon oxynitride phase (the Si–N–O fibre),[21] a silicon oxycarbide continuum involving interconnected nanocrystalline SiC and amorphous silicon oxycarbide phases[22–24] (like in the Si–C–O fibre) or a single nanocrystalline SiC phase (like in the Si–C fibre). The concept of silicon oxycarbonitride continuum which has been described in previous studies is based on detailed chemical analyses such as ^{29}Si-MAS-NMR, XPS, EELS, IR, EPMA and elemental analyses.[21,22–24] The general assumptions for the calculation of the chemical composition of the Si–C–N–O continuum are essentially : (i) the tetrahedral coordination of all the Si atoms (with C, N and O atoms as first neighbours), (ii) the C–Si_4 tetrahedral environment of the C atoms involved in the continuum only, (iii) the N–Si_3 environment of all the N atoms and (iv) the O–Si_2 environment of all the O atoms. If $Si-C_xN_YO_{(4-X-Y)}$ $(0 \leqslant X \leqslant X+Y \leqslant 4)$ is the average tetrahedral environment of silicon atoms in the Si–C–N–O continuum (Fig. 2), the chemical atomic composition of the later material becomes $Si-C_{X/4}N_{Y/3}O_{(4-X-Y)/2}$ $(0 \leqslant X \leqslant X+Y \leqslant 4)$ or, with $x = X/4$ and $y = Y/4$ $(0 \leqslant x \leqslant x+y \leqslant 1)$ $SiC_xN_{4y/3}O_{2(1-x-y)}$, where x, y and $1-x-y=z$ are the average fractions of, respectively, the number of Si–C, Si–N and Si–O bonds to the total number of Si–i bonds (i = C,N,O), i.e. $x = n_{Si-C}/\Sigma_i n_{Si-i}$, $y = n_{Si-N}/\Sigma_i n_{Si-i}$ and $z = n_{Si-O}/\Sigma_i n_{Si-i}$ (i = C,N,O). The parameters x and y, which define the composition of the continuum, as well as the free carbon concentration c_{Cf} are directly related to the average composition of the fibre, according to: $x = 1 - 3c_N/4c_{si} - c_O/2c_{si}$, $y = 3c_N/4c_{si}$ $c_{Cf} = c_C - c_{si} + 3c_N/4$. Hence, the phase composition of the Si–C–N–O fibres is defined by three parameters (x, y and c_{Cf}) of which only two, x and y, fully describe the composition of the Si–C–N–O continuum and one, c_{Cf}, the concentration of free carbon. In the Si–C–O system, two

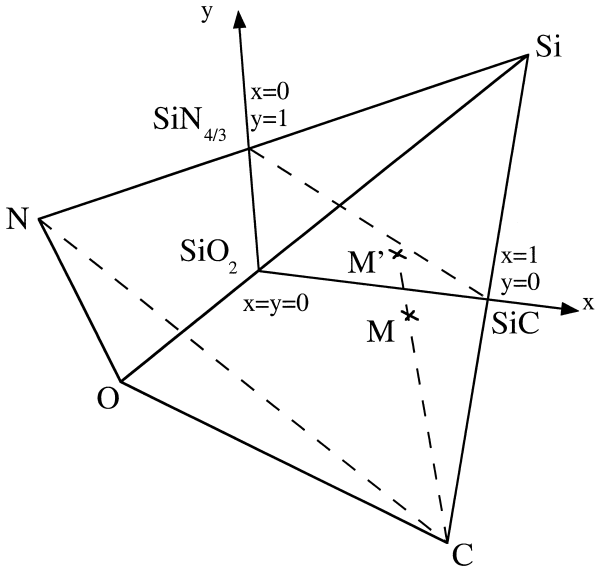

Fig. 1. Quaternary diagram showing the composition of the Si–C–N–O fibres.

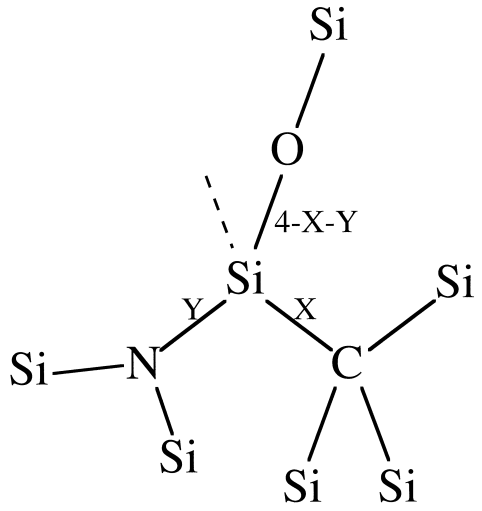

Fig. 2. Schematic description of the Si–$C_XN_YO_{4-X-Y}$ $(0 \leqslant X \leqslant X+Y \leqslant 4)$ tetrahedral environment of silicon atoms in Si–C–N–O ceramics.

parameters, x and c_{Cf}, are needed to define the phase composition whereas only one, y, is required in the case of the Si–N–O system, where the Si–N–O continuum is the only phase involved.[21] The values of x, y and c_{Cf} are plotted in Fig. 3, in a composition quaternary diagram.

3.2. Oxidation behaviour

Small diameter fibres are particularly suitable for the investigation of oxidation kinetics through TGA experiments because of their high and uniform specific surface (due to their small and regular diameter) and the limited contact points preventing the coalescence of the viscous oxide layer (as opposed to fine powders).

The change of the relative weight of the fibres during an oxidation test is related to their oxidation rate and more especially within the passive regime, to the growth of an oxide layer at their surface. A weight increase was generally observed for all the fibres within the whole tested temperature range, whose rate increased as the temperature was raised. The TGA curves (the relative weight $\Delta m/m_0$, versus time) are generally parabolic for $T \leqslant 1400°C$ (Fig. 4) except for the Si–C–O fibre beyond 1200°C and for the Si–Ti–C–(O) fibre beyond 1350°C. Above these temperature limits, a catastrophic increase of $\Delta m/m_0$ was observed and the parabolic regime was no longer observed.

SEM analyses of the oxidized specimens confirmed the presence of the oxide scale resulting from oxidation. For low temperatures, when the oxidation rate is particularly low and the oxide layer and the underlying substrate are very adherent (e.g. for the Si–C–N–O and the Si–N–O fibres), the thickness of the oxide layer, e, could not be reliably measured from direct secondary electrons SEM imaging. In such a case, back-scattered electrons imaging was used (see example in Fig. 5). A short bleaching in a HF aqueous solution was even sometimes necessary to reveal the ceramic/oxide interface to measure e.

For all the fibres, the oxide scale remains dense and adherent to the substrate for $T \leqslant 1400°C$, except for the Si–C–O fibre at 1300°C and for the Si–Ti–C–(O) fibre at 1400°C.

Within this temperature range, the continuous oxide apparently acts as a passivating scale owing to two main reasons: (i) the ceramic/oxide conversion is always associated to a volume expansion, i.e. the ratio Δ representing the volume of the oxide formed per volume of the ceramic consumed is always greater than 1 (equation 1, Table 3) and (ii) the oxide formed is sufficiently plastic, both factors increasing its capability of covering the ceramic substrate in a continuous manner.

$$\Delta = \frac{M_{SiO_2}}{M_{Si}} \frac{d}{d_{SiO_2}} C_{Si} \quad (1)$$

After oxidation beyond 1400°C, the oxide formed at the surface of the Si–C–O and Si–Ti–C–(O) fibres is

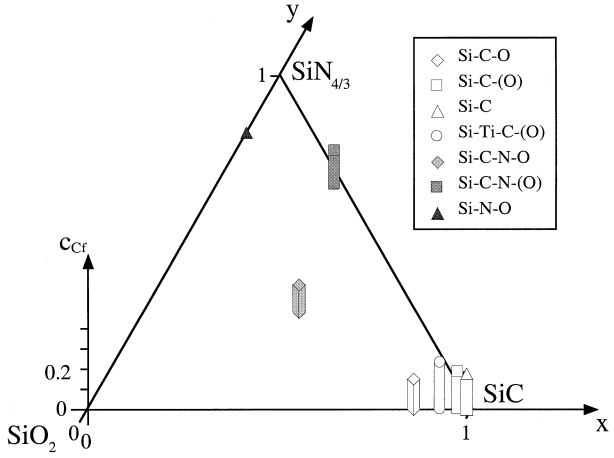

Fig. 3. Composition diagram showing the free carbon concentration (c_{Cf}) and the fraction of C and N bonds to silicon (respectively x and y).

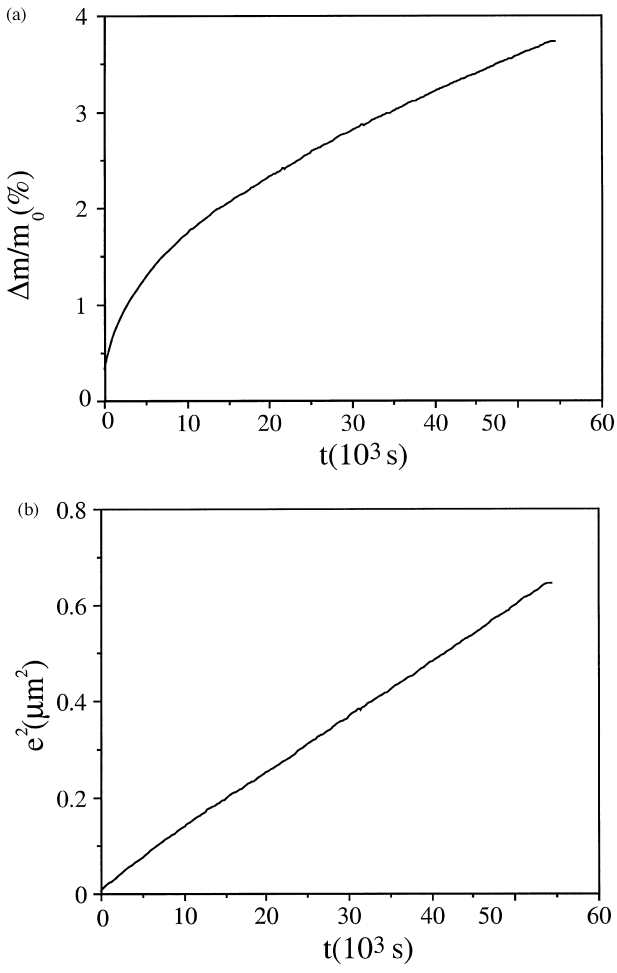

Fig. 4. : Oxidation kinetics of Si–C–N–(O) fibres in pure oxygen ($P = 100$ kPa) at 1400°C. (a) relative weight versus time and (b) square of the oxide thickness versus time.

Table 3
Weight gain/oxide thickness conversion factor (F_C) and volume change ratio (Δ) calculated for the oxidation of the Si–C–N–O fibres

	d(gcm^{-3})	r_0(μm)	$S_0(m^2g^{-1})$	C_{si}(wt.%)	F_C	Δ
Si–C–O	2.56	7.5	–	58.8	2.82	1.47
Si–C–(O)	2.73	6.5	–	60.5	2.71	1.61
Si–C	2.77	7.0	–	60.5	2.75	1.63
Si–Ti–C–(O)	2.37	6.0	–	55.0	2.96	1.29
Si–C–N–O	2.45	10.0	–	53.3	4.47	1.27
Si–C–N–(O)	2.64	6.0	–	56.0	3.60	1.44
Si–N–O	3.00	–	0.45	57.2	3.70	1.67
SiC	3.20	–	–	70.0	–	2.18
Si_3N_4	3.20	–	–	60.0	–	1.87

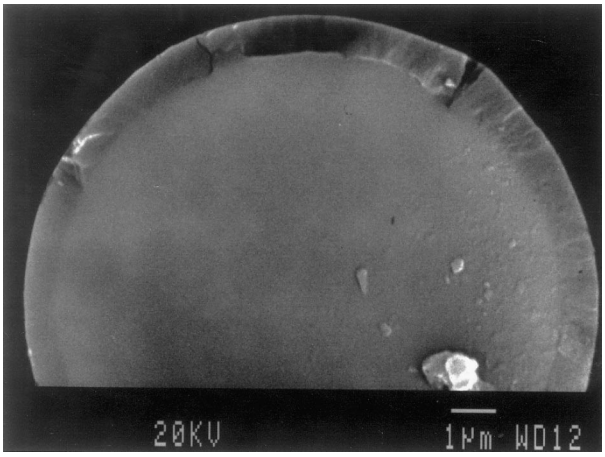

Fig. 5. SEM micrograph of a Si–C–N–(O) fibre oxidised 15 h in pure oxygen ($P = 100$ kPa) at 1400°C.

extremely thick and no longer continuous nor adherent to the substrate. It shows extensive cracking, with sometimes debonding of the oxide and irregular oxidation patterns, with porous oxide at the fibre/oxide interface. This phenomenon is related to the increase of the oxidation rate recorded by TGA. For the other fibres, some cracks occasionally appear in the oxide scale at $T = 1400$°C, although it is still dense and adherent. These cracks are thought to occur on cooling. They might result from the thermal expansion mismatch between the silica and the fibres, or the density change related to the β-α cristoballite transition occurring on cooling, while the plasticity of the oxide is too high to relax strain. However, very few cracks are also likely to originate at high temperature. They are only observed when the oxide is substantially crystalline, i.e. for $T \geqslant 1400$°C. The oxide cracking results in an inhomogenous oxide thickness at the vicinity of the crack tips (Fig. 5), but their number is so limited that the parabolic regime is still observed by TGA.

The chemical composition of the oxide scale was also investigated. From the surface to the interfacial zone, AES and EELS analyses of the oxide layer formed at the surface of the fibres only evidenced silicon and oxygen atoms (except for the Si–Ti–C–(O) fibre), with a composition close to SiO_2. No carbon nor nitrogen traces were detected throughout the oxide layer.[21,33,65–66]

Under the following assumptions, the thickness of the oxide layer can be easily inferred from $\Delta m/m_0$. Assuming that (i) the oxide formed during oxidation is pure and dense silica [the low amounts of titanium in the oxide layer formed at the surface of the Si–Ti–C–(O) fibres can be reasonably neglected, since the Ti/Si atomic ratio is below 3%], (ii) that the density and the bulk composition of the fibre are unchanged (as supported by EPMA) and (iii) for small oxide thicknesses ($e << r_0$), e, can be written according to the following equation:[33,66]

$$e = r_0 F_c \frac{\Delta m}{m_0} \tag{2}$$

where

$$F_c = \frac{1}{2} \frac{M_{SiO_2} C_{Si}}{M_{SiO_2} C_{Si} - M_{Si}} \frac{d}{d_{SiO_2}} \tag{3}$$

where F_c is a dimensionless conversion factor and r_0, M_{Si}, M_{SiO_2}, d, d_{SiO_2} and C_{Si} are respectively the radius of the fibre, the molar masses of silicon and silica, the densities of the fibre and pure silica and the silicon weight concentration of the fibre (Table 3). Alternatively, when the average radius of the fibres was too dispersed to be measured (e.g. for the Si–N–O fibres), the silica thickness was assessed from their specific surface S_0 measured by BET, according to equation :

$$e = \frac{1}{S_0 d_{SiO_2}} \frac{M_{SiO_2} C_{Si}}{M_{SiO_2} C_{Si} - M_{Si}} \frac{\Delta m}{m_0} \tag{4}$$

The silica thicknesses were also directly measured by SEM analysis after the test in order to validate Eq. (2). A good agreement was found between the calculated and the measured values (Table 4). The silica thickness obeys a parabolic law versus time which can be written as:

$$e^2(t) - e_0^2 = K_T t \tag{5}$$

where K_T is the kinetic constant at temperature T and e_0 is the thickness of the silica layer for $t = 0$. The K_T values for the different fibres are presented in Table 5. The thermal dependence of the oxidation kinetic constants K_T of the various fibres are represented in an Arrhenius plot, along with the values obtained for high purity monocrystalline and polycrystalline (CVD) SiC and Si_3N_4 which have been reported in the literature (Fig. 6). For a given material and within the studied temperature range, K_T obeys an Arrhenius law:

Table 4
Oxide thicknesses formed at the surface of the Si–C–N–O fibres in pure oxygen versus temperature and time, as measured by SEM (e_m) and calculated from the weight gains (e_c)

T(°C)				1000		1100	1200	1300	1350	1400
Si–C–(O)	t(h)			11		–	–	–	–	7
	e_m(μm)			0.25		–	–	–	–	0.63
	e_c(μm)			0.29		–	–	–	–	0.65
Si–C	t(h)	10			20	15	15	15	–	15
	e_m(μm)	0.25			0.35	0.45	0.65	0.80	–	1.1
	e_c(μm)	0.24			0.35	–	0.59	–	–	1.1
Si–Ti–C–(O)	t(h)			–		20	–	10	10	–
	e_m(μm)	–				0.50	–	0.70	0.90	–
	e_c(μm)	–				0.45	–	0.67	0.79	–
Si–C–N–O	t(h)			200		–	50	–	–	20
	e_m(μm)			0.60		–	0.80	–	–	1.0
	e_c(μm)			0.53	–	–	0.78	–	–	1.13
Si–C–N–(O)	t(h)			0.50		15	0.20	0.15	–	15
	e_m(μm)			0.1	–	–	0.30	0.55	–	0.85
	e_c(μm)			–		0.07	0.29	0.59	–	0.81
Si–N–O	t(h)			–	–	–	–	–	–	10
	e_m(μm)			–		–	–	–	–	0.59
	e_c(μm)	–		–	–	–	–	–	–	0.75

Table 5
Parabolic law kinetic constants (K_T) for the oxidation of the Si–C–N–O fibres in pure oxygen

	K_T(nm^2s^{-1})								
T(°C)	800	1000	1100	1150	1200	1250	1300	1350	1400
Si–C–O	0.50	1.4	2.4	–	4.8	–	–	–	–
Si–C–(O)	–	2.0	–	–	6.9	–	11.0	–	17.0
Si–C	0.27	1.8	–	–	6.2	–	–	–	21.0
Si–Ti–C–(O)	–	2.3	2.9	–	5.3	–	12.0	–	17.0
Si–C–N–O	–	0.37	1.0	–	3.1	–	–	–	14.8
Si–C–N–(O)	–	0.013	0.098	–	1.4	–	6.4	–	11.8
Si–N–O	–	–	0.013	0.035	0.36	0.80	1.6	8.2	15.6

$$\ln K_T = \ln K_\infty - \frac{E_a}{RT} \quad (6)$$

where K_∞ is a pre-exponential parameter, R the ideal gas constant and E_a the apparent activation energy (Table 6).

3.2.1. Fibres from the Si–C–O system and sub-systems

The different Si–C–O fibres generally exhibit a parabolic time-dependence of oxidation within the range 800–1400°C. The parabolic rates for a given temperature are all close to the value for pure SiC. The corresponding activation energies all fall within the range 70–110 kJ mol^{-1}, also in agreement with the values reported for SiC (E_a = 90 to 140 kJ mol^{-1}).[38,42,61] However, the oxidation kinetics dramatically increase and the parabolic law is ruled-out for the Si–C–O and the Si–Ti–C–(O) fibres, respectively for $T > 1200$°C and $T > 1350$°C. It is worthy of note that within the parabolic regime, both the free carbon concentrations (c_{Cf}) and ratio of O bonds to Si ($z = 1 - x - y$), have no significant influence on the parabolic rates.

3.2.2. Fibres from the Si–C–N–O and Si–N–O systems

The oxidation behaviour in these systems considerably differs from that of SiC. The parabolic constants of oxidation are generally lower than those of SiC, especially at low temperature ($T < 1400$°C). The corresponding activation energies are significantly higher, i.e. E_a = 165, 319 and 464 kJ mol^{-1}, respectively for the Si–C–N–O, the Si–C–N–(O) and the Si–N–O fibres. The magnitude of the parabolic constants as well as the activation energies ranges from that reported for SiC (E_a = 90 to 140 kJ mol^{-1}) to that for Si_3N_4 (E_a = 330 to 490 kJ mol^{-1}).[46–49,61] Like for the Si–C–O fibres, the oxygen and the free carbon concentrations have a limited influence on the oxidation rates. Conversely, the parameters x and y, i.e. the ratios of C and N bonds to Si, respectively, have obviously a prevalent effect. Indeed, K_∞ and E_a vary continuously and almost linearly from the values for SiC ($y/(x+y) = 0$) to those for Si_3N_4 ($y/(x+y) = 1$) whatever the $z = 1 - x - y$ and c_{Cf} values (Fig. 7).

4. Discussion

SiC and Si_3N_4 actually set the two composition bounds of the ternary diagram describing the ratio of C, N, and O bonds to silicon (Fig. 3). Their respective oxidation behaviours were not investigated here but they are well documented in the literature. Though

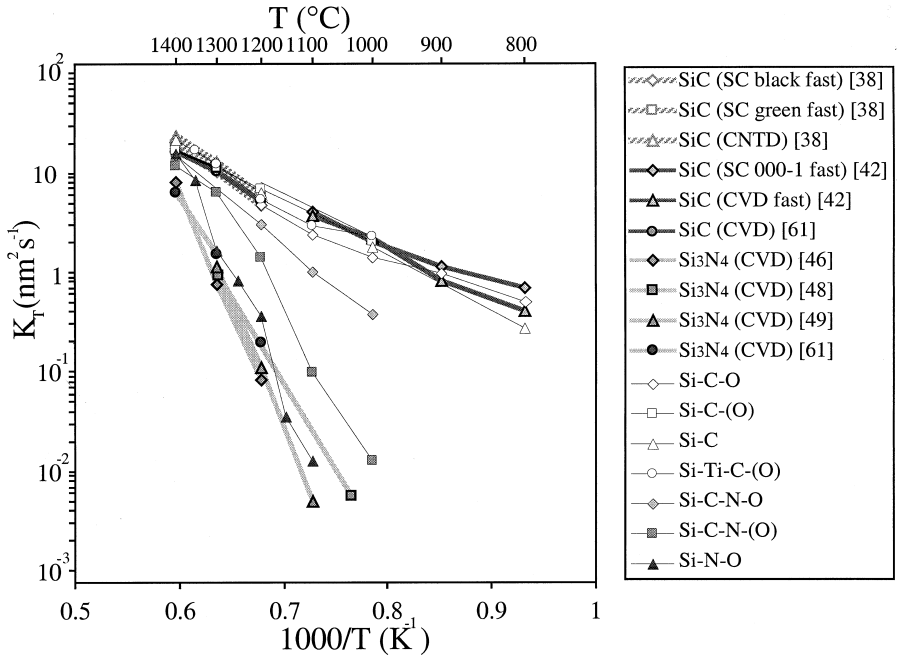

Fig. 6. Oxidation parabolic kinetic constants (K_T) in pure oxygen ($P = 100$ kPa) of the Si–C–N–O fibres and crystalline compounds.

Table 6
Arrhenius law constants (E_a and ln K_∞) of the parabolic law kinetic constants (K_T) for the oxidation of the Si–C–N–O fibres in pure oxygen

	E_a (kJ mol$^{\pm 1}$)	ln K_∞ ($nm^2 s^{-1}$)	x ($0 \leqslant x \leqslant 1$)	y ($0 \leqslant y \leqslant 1$)	$z = 1-x-y$ ($0 \leqslant z \leqslant 1$)	c_{Cf} (at.%)	α
Si–C–O	70±7	−6.7±0.7	0.85	0	0.15	15.0	1.46
Si–C–(O)	95±1	−4.2±0.1	0.96	0	0.04	18.5	1.67
Si–C	107±3	−3.2±0.3	0.99	0	0.01	17.5	1.70
Si–Ti–C–(O)	101±15	−3.7±1.3	0.92	0	0.08	23.0	1.69
Si–C–N–O	165±5	0.8±0.4	0.40	0.29	0.31	13.5	1.08
Si–C–N–(O)	319±27	12.1±2.2	0.30	0.68	0.02	15.8	1.34
Si–N–O	464±27	22.4±2.2	0	0.83	0.17	0	0.83
SiC [3,5,6]	90/140	−5.1/−0.5	1	0	0	0	1.5
Si_3N_4 [6,7,8,9]	33/490	11.6/23.5	0	1	0	0	1

having common main features, i.e. the formation of a protective silica scale (passive oxidation), their kinetics and temperature dependence differ greatly as well as the mechanisms involved.[37–62] One can, therefore, expect that the oxidation properties of more complex Si–C–N–O materials strongly depend on their composition, while being bounded by those of SiC and Si_3N_4. It is also thought that the oxidation mechanisms in such systems have common features with those of SiC and Si_3N_4. The experimental studies clearly evidenced that, similarly to SiC and Si_3N_4, all the Si–C–N–O ceramics studied here exhibit a parabolic rate of oxidation whose kinetics are likely to be controlled by diffusion phenomena. An important result established here is that the parabolic constants K_T at a given temperature and the activation energy E_a of the various ceramics vary consistently with parameters x and y which precisely define the ratio of C and N bonds to Si atoms in the material, from the values for SiC ($x = 1$, $y = 0$) to those for Si_3N_4 ($x = 0$, $y = 1$) (Fig. 7). The mechanisms responsible for the oxidation of SiC and Si_3N_4 are therefore likely to be partly involved in the oxidation of more complex ceramics from the Si–C–N–O system.

4.1. The Si–C–O system and related sub-systems

The oxidation of pure SiC (i.e. SiC single crystal or polycrystalline SiC-CVD) generally results in the formation of a pure homogeneous silica scale, according to the equation:

$$SiC_{(s)} + 3/2O_{2_{(g)}} \rightarrow SiO_{2(s)} + CO_{(g)} \quad (7)$$

The controlling step imposing the oxidation rate for SiC below 1400°C, is generally admitted to be the permeation of O_2 through the silica scale inward. This

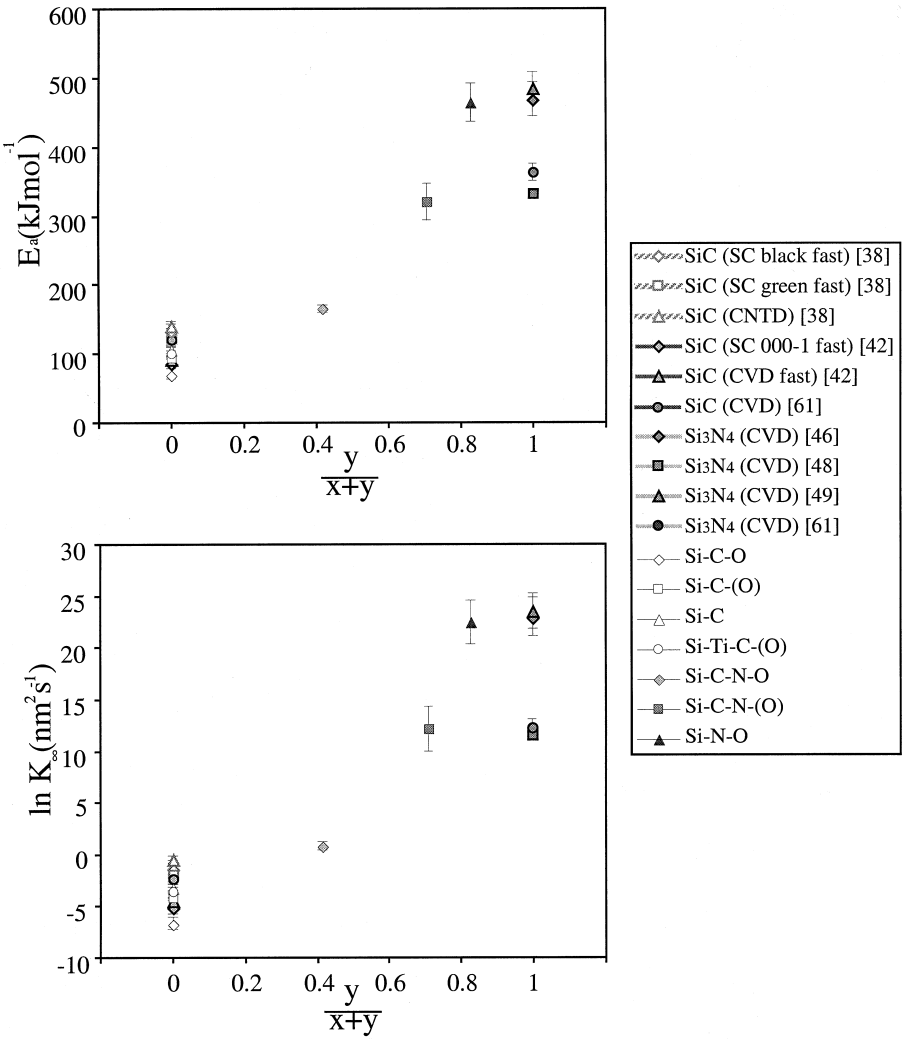

Fig. 7. Arrhenius law parameters (E_a and ln K_∞) of the oxidation parabolic kinetic constants of the Si–C–N–O fibres and crystalline compounds.

assumption is based on the following remarks : (i) similarly to pure silicon, the oxidation rate of SiC is parabolic suggesting a diffusion phenomenon as rate controlling, (ii) K_T and E_a values are essentially the same as those for silicon after taking into account the additional oxygen needed to oxidise carbon,[38,58–59] (iii) K_T is dependent on the oxygen partial pressure,[39–40] (iv) CO has been concluded to diffuse readily outward[39,59] and (v) a single interfacial reaction controlling step is very improbable because the oxidation rate is not linear but parabolic. Hence, though a mixed control mechanism involving both diffusion (either O_2 inward or CO outward) and interfacial reaction is not excluded,[60] most of the data for pure SiC suggest the oxygen permeation through the silica layer as being the rate controlling step. It is, however, worth mentioning that Costello et al. reported that the Si (0001) face of a SiC single crystal exhibits significantly lower parabolic oxidation rates and a higher activation energy than the C (000-1) face.[38] More recently, the same conclusions were reported by Ramberg et al. and extended to highly textured CVD-SiC.[41–42] This behaviour was suggested to arise from the presence of a Si–C–O sublayer appearing only for the slow oxidation rate faces of the SiC single crystal and the CVD-SiC film. This sublayer, more resistant to oxygen diffusion, would result in much lower parabolic constants than on the opposed faces.

All the materials described in this study have an isotropic microstructure (either amorphous or nanocrystallized). Their oxidation behaviour is therefore expected to be dominated by the highest oxidation rate of SiC monocrystals (that of the C-face), consistently with the large majority of the data obtained for similar materials.

The magnitude of the oxidation parabolic rates obtained for the different Si–C–O fibres are generally close to those reported for crystalline SiC and the corresponding activation energies fall all within the range 70–110 kJ mol^{-1}, close to the values for SiC.[38,42,61] This feature suggests that, similarly to pure SiC, the oxidation kinetics of the Si–C–O fibres is controlled by the same mechanism as that of the oxidation of silicon, i.e.

the permeation of molecular oxygen inward through the growing silica layer. The general oxidation reactions for the Si–C–O fibres can be written as follows:

$$SiC_xO_{2(1-x)_{(s)}} + 3/2_xO_{2_{(g)}} \rightarrow SiO_{2(s)} + xCO_{(g)} \quad (8)$$

with $0 \leqslant x \leqslant 1$ for the $SiC_xO_{2(1-x)}$ continuum and

$$C_{(s)} + 0.5\ O_{2(g)} \rightarrow CO_{(g)} \quad (9)$$

for the free carbon phase. The reactions corresponding to Eqs. (8) and (9) are independent but simultaneous and their ratio for 100 average atoms of ceramic oxidised is defined by the overall equation :

$$(10) = 100(1 - c_{Cf})/(3 - x)(8) + 100c_{Cf}(9) \quad (10)$$

The equations are basically the same for the Si–Ti–C–(O) fibre, except the presence of low amounts of Ti atoms substituting to Si atoms (the oxidation number and the chemical environment being the same) in the oxycarbide continuum and in the silica scale (about 2% of Ti are substituted for Si sites).

The oxidation of the Si–C–O fibres differs from that of pure SiC in the presence of the free carbon, necessitating an additional oxygen flux to be oxidised (an addition of $c_{Cf}(3 - x)/(1 - c_{Cf})$ mol to the 1.5 mole of O_2 needed to yield 1 mol of SiO_2) and oxygen atoms in the oxycarbide phase, conversely requiring a lesser oxygen flux ($1.5x$ mol of O_2 instead of 1.5 mol). Assuming that the permeation of O_2 through silica is still the rate limiting step for the oxidation of the Si–C–O fibres, the parabolic rate should therefore depend on the stoichiometry of the material. To take this into account, a parameter α, i.e. the number of mol of O_2 needed to oxidise the material into 1 mol of SiO_2, can be introduced.[60] Under the above assumption, the αK_T value should be constant for all the Si–C–O materials, α being equal to 1 for silicon, 1.5 for SiC and more generally $\alpha = 1.5x + c_{Cf}(3 - x)/(1 - c_{Cf})$ for the Si–C–O fibres. The α values of the latter are presented in Table 6. It is worthy of note that no significant difference in α is observed for the different materials (α ranges from 1.5 to 1.7). Consequently, both the oxygen concentration and the free carbon (though present in relatively high amounts) cannot be expected to affect significantly the parabolic oxidation rates with respect to pure SiC. The variations of K_T which might be assigned to the stoichiometry should actually hardly exceed the experimental error due to the TGA measurement and the K_T calculation. Accordingly, the effect of the composition of the Si–C–O fibres (within the present range of x and c_{Cf} values) was not evidenced by TGA.

If the amount of oxygen and free carbon in the fibres only slightly affects the oxidation parabolic rates, as long as a parabolic time dependence is observed, it has a dramatic influence on the upper temperature limit beyond which the parabolic regime is no more obeyed. This behaviour is likely to be related to the chemical and the structural instability of these fibres reported at high temperatures in inert atmosphere. It is well established that the oxycarbide phase present in the fibres is metastable and intrinsically decomposes in inert atmosphere at high temperature (beyond 1200°C) into crystalline SiC and SiO and CO gaseous species.[27–29,34] The decomposition finally yields a SiC grain coarsening, an emission of SiO and CO (whose extent is related to x) and eventually residual free carbon (whose amount depends on x and c_{Cf}). Though in a lesser extent, the same phenomenon is likely to occur despite the apparent passive oxidation regime. The intrinsic decomposition of the fibres is thought to be responsible for the dramatic increase of the oxidation rate becoming no longer parabolic at high temperature. This assumption is supported by the presence at the fibre/oxide interface of a highly inhomogeneous and porous zone. Some debonding at the interface was sometimes also observed.[65] The pores in the silica at the interface might originate from the pressure build-up of the gaseous species (mainly CO) resulting from the decomposition of the oxycarbide. Although the fast CO diffusion outward, preventing the formation of bubbles at the SiC/SiO_2 interface for the oxidation of stoichiometric SiC, the considerably higher CO partial pressure resulting from the oxycarbide decomposition might be sufficient to allow the formation of pores within the silica and at the fibre/oxide interface. The pressure resulting from gaseification would blow up the dense outer scale generating radial cracks and fibre/oxide debonding. Under these conditions, the micro-cracked oxide scale is no longer protective and allows a fast oxygen diffusion inward to the interface, resulting in a dramatic increase of the oxidation rate. This phenomenon is not observed for the Si–C–(O) nor the Si–C fibres, which are chemically stable at high temperature in inert atmosphere 11–33 but only for the Si–C–O and the Si–Ti–C–(O) fibres, both rich in oxycarbide phase are therefore highly unstable,[27–29,34] respectively for $T > 1200$°C and $T > 1350$°C.

Furthermore, hydrogen, which is present in small amounts in the Si–C–O fibres (especially in the Si–C–O and Si–Ti–C–(O) fibres), might also affect the oxidation regime. The fibres prepared at relatively low temperatures (1100–1300°C) contain up to several atomic percents of hydrogen which is released when annealed at higher temperatures.[24] Although H_2O is generally reported to enhance the oxidation rate of silicon carbide,[62] this effect is not fully understood yet. It might effect the physical properties of the oxide (viscosity, porosity,...), for instance through the formation of OH species, favouring the permeation of O_2.[47] Hydrogen or water vapour might also enhance the devitrification of

silica. Whereas the crystallisation of SiO_2 is generally observed from around 1400°C,[38] it starts at a temperature as low as 1200°C for the Si–C–O fibres.[33–65] However the effect of devitrification on the O_2 permeation and, therefore, the oxidation rate remains unclear. Simultaneously to the oxidation process, a release of hydrogen from the fibre bulk occurs beyond 1200°C.[24–34] This phenomenon might also be partly responsible for the deviation to the parabolic rate and the Arrhenius law observed for the Si–C–O and the Si–Ti–C–(O) fibres. Conversely, the most thermally stable fibres, i.e. the Si–C–(O) and the Si–C fibres, were found to exhibit oxidation parabolic rates and an activation energy similar to those for pure SiC within the whole 800–1400°C temperature range. It is worthy of note that these fibres were processed at temperatures above 1350–1400°C.[11–33] As a consequence, no intrinsic decomposition (owing to the absence of oxycarbide phase) nor hydrogen emission (being mostly eliminated during the high temperature processing) are expect to affect the oxidation rate within that test temperature range.

A significant increase of the activation energy for SiC was reported in the literature beyond 1350–1400°C.[38–39] It was concluded to arise from the change of the oxygen diffusion regime from molecular permeation at low temperature, to network exchange diffusion beyond 1400°C. The present experimental data tend to show that the permeation of O_2 remains the prevalent mechanism up to at least 1400°C for the most stable fibres.

As already mentioned, a crystallisation of the SiO_2 layer is observed, very limited at a temperature of 1200°C but rapidly improving at higher temperatures. After 10 h at 1400°C, the oxide is substantially crystalline. A short bleaching in an HF aqueous solution allows the crystobalite domains to be distinguished from the amorphous silica. An examination of the section of the oxidised/HF etched fibres did not evidence any change in the thickness of the oxide nor any discontinuity in the fibre/oxide interface, from amorphous to crystalline oxide domains. This feature, as well as the constant activation energy, indicates that the oxidation rate is approximately independent on the crystalline state of the oxide and would suggest a value of the oxygen diffusivity in crystobalite similar to that in amorphous SiO_2. Assuming that the permeation of oxygen is rate controlling, because of its stiffer and denser structure, one would expect a slower diffusion rate in cristoballite than in amorphous SiO_2. Unfortunately, oxygen diffusivity data are still scarce and sometimes contradictory to clarify this point. It is, however, worth mentioning that the crystallisation of SiO_2 seldom indirectly results in local inhomogeneous oxidation pattern. The strain build-up resulting from the volume change due to oxidation and crystallisation, as well as the increase of the viscosity of the oxide, result in radial and interfacial cracks locally favouring the oxidation.

4.2. The Si–C–N–O, Si–N–O and Si–N systems

The oxidation behaviour of Si_3N_4 presents a number of common features with that of SiC. The oxidation results in the formation of an oxide layer consisting mainly of pure silica. The corresponding reaction is represented by the following equation.

$$Si_3N_{4(s)} + 3\ O_{2(g)} \rightarrow 3SiO_{2(s)} + 2N_{2(g)} \quad (11)$$

However, some authors proposed a more complex process consisting in the two successive equations [such as (11) = (12) + 1.5 (13)]:

$$Si_3N_{4(s)} + 3/4O_{2(g)} \rightarrow 3/2\ Si_2N_2O_{(s)} + 0.5N_{2(g)} \quad (12)$$

and

$$Si_2N_2O_{(s)} + 3/2O_{2(g)} \rightarrow 2SiO_{2(s)} + N_{2(g)} \quad (13)$$

The oxidation results in the formation of a duplex Si_2N_2O/SiO_2 layer where the silicon oxynitride sub-layer is not crystalline nor necessarily stoichiometric.[46,47,52–59] A direct evidence (SIMS, TEM, XPS, AES, RBS) of the existence of such a silicon oxynitride sub-layer has been established[46,52–55]. It is also supported by indirect investigations such as optical measurements and step-by-step etching.[46]

Similarly to SiC, Si_3N_4 generally exhibits a parabolic oxidation rate where kinetic constants K_T, are dependent on the oxygen partial pressure while independent on the nitrogen partial pressure.[46] Like for silicon carbide, the interfacial reaction as rate-limiting step is improbable since no linear oxidation rate was observed. A controlling step similar to the one involved for SiC, i.e. the diffusion of oxygen through the oxide layer, is therefore likely to impose the oxidation rate. However, a simple comparison in a Arrhenius plot of the SiC and Si_3N_4 parabolic rate constants obviously demonstrates different magnitudes and temperature dependencies. Whereas K_T values for Si_3N_4 are close to the SiC values around 1400°C, they become significantly lower as the temperature decreases. Indeed, the corresponding activation energies typically range 330–490 kJ mol^{-1} for Si_3N_4 while only 90–140 kJ mol^{-1} for SiC. Hence, if the permeation of O_2 through SiO_2 governs the oxidation rate of Si and SiC, it seems to be ruled out for Si_3N_4. The silica scale formed on Si, SiC and Si_3N_4 has apparently the same nature. Additionally, the N_2 diffusion outward has no apparent effect on the oxidation rate, since K_T is not dependent on P_{N_2}. The oxygen transport mechanism through the SiO_2 outer layer is therefore probably the same for Si_3N_4 as for Si and SiC. The

higher activation energy for Si_3N_4 has been attributed to the oxygen transport through the silicon oxynitride layer. Du et al. proposed a lower permeability to oxygen of this sub-layer than SiO_2.[46–47] The silicon oxynitride layer acting as a diffusion barrier and gradually increasing in thickness during oxidation would give rise to lower parabolic rates and a higher activation energy than those for SiC. However, this assumption presents some thermodynamic inconsistencies for the oxygen diffusion as rate controlling.[51,58,60] Alternatively, Luthra proposed a mixed interfacial reaction and nitrogen diffusion mechanism as rate controlling.[51,60] Such mechanism would solve the discrepancies encountered by Du et al. while giving rise to oxidation rates approaching a parabolic dependence. Finally, the oxidation kinetics of Si_3N_4 were modelled describing a simultaneous oxygen diffusion/reaction through the oxynitride sublayer with a depth-variable composition.[56–57] This concept of gradual substitution of O for N atoms in the oxynitride instead of interfacial reactions is attractive because it overcomes the thermodynamic inconsistencies (thermochemical calculations at equilibrium become inadequate since the oxidation is not, in this case, strictly diffusion-controlled) and accounts for the graded composition of the sublayer. However, owing to the complexity of such process, the model for the oxidation kinetics still has some limitations and needs some further developments (especially in terms of temperature dependence).

The oxidation of ceramics from the Si–C–N–O system is particularly complex because it combines the oxidation features of SiC and Si_3N_4, e.g. the simultaneous diffusion of CO and N_2 through the oxide layer outwards. It also involves a free carbon phase whose oxidation results in an additional CO flux, some oxygen initially present in the ceramic and possibly some traces of hydrogen. Neglecting the presence of hydrogen, the overall reaction of the oxidation can be described by the following equation :

$$SiC_xN_{4y/3}O_{2(1-x-y)_{(s)}} + (3x/2 + y)O_{2(g)} \rightarrow SiO_{2(s)} + xCO_{(g)} + 2y/3N_{2(g)} \quad (14)$$

(with $0 \leqslant x \leqslant x + y \leqslant 1$) for the $SiC_xN_{4y/3}O_{2(1-x-y)}$ continuum and in some cases :

$$C_{(s)} + 1/2\ O_{2(g)} \rightarrow CO_{(g)} \quad (15)$$

for the free carbon phase. The overall equation for 100 average atoms is therefore :

$$(16) = 100(1 - c_{Cf})/(3 - x - 2y/3)(14) + 100c_{Cf}(15) \quad (16)$$

The parameter α (the number of mole of O_2 needed to form one mole of SiO_2) becomes then:

$$\alpha = 1.5x + y + 0.5c_{Cf}(3 - x - 2y/3)/(1 - c_{Cf}) \quad (17)$$

(Table 6). α ranges from 0.83 for fibres with high z and low x and c_{Cf} values (e.g. the Si–N–O fibre), to 1.34 for fibres with low z and high x and c_{Cf} values [e.g. the Si–C–N–(O) fibre].

Similarly to the Si–C–O systems, one of the significant features of the oxidation behaviour of the various Si–C–N–O systems, is the moderate influence of the oxygen and the free carbon concentrations. Conversely, the effect of x and y is indeed determinant on the values of E_a and K_∞. On the basis of the oxidation mechanism of Si and SiC (i.e. the permeation of O_2 through the SiO_2 scale inwards), the expectable effect of z, c_{Cf} and α on the K_T values is limited and under no circumstances supposed to affect the rate limiting step nor the activation energy E_a.

The experimental data presented here strongly suggest that the oxidation mechanism and its rate limiting step, change continuously from those for SiC (for $x = 1$ and $y = 0$), to those for Si_3N_4 (for $x = 0$ and $y = 1$), consistently with the E_a and the K_∞ values. It is proposed that the oxidation process of Si–C–N–O ceramics involves a simultaneous (i) oxygen diffusion inwards, (ii) reaction and (iii) CO and N_2 diffusion outwards through a silicon oxycarbonitride continuum sub-layer of a graded composition ranging from SiO_2 (at the free surface) to the bulk composition (Fig. 8). The gradual increase of the oxidation rate, either with time at a given depth, or along the thickness of the sub-layer for a given time, corresponds to a continuous substitution of Si–O bonds for both the Si–C and Si–N bonds of the $SiC_xN_{4y/3}O_{2(1-x-y)}$ continuum. The oxidation reaction of the latter phase is, therefore :

$$SiC_xN_{4y/3}O_{2(1-x-y)_{(s)}} + (3\delta x/2 + \delta y)O_{2(g)} \rightarrow SiC_{(x-\delta x)}N_{4(y-\delta y)/3}O_{2(1-x-y+\delta x+\delta y)_{(s)}} + \delta xCO_{(g)} + 2\delta y/3\ N_{2(g)} \quad (18)$$

($0 \leqslant \delta \leqslant x$ and $o \leqslant \delta y \leqslant y$) and is combined to the combustion of the free carbon phase:

$$\delta c_{Cf}C_{(s)} + \delta c_{Cf}/2\ O_{2(g)} \rightarrow \delta c_{Cf}CO_{(s)} \quad (19)$$

($0 \leqslant \delta c_{Cf} \leqslant c_{Cf}$). This oxidation process has some common features with the mechanism suggested by Sheldon et al. and Ogbuji et al. for the oxidation of Si_3N_4, e.g. the simultaneous oxygen diffusion/in-depth reaction within a sub-layer of continuously variable composition and structure.[56,57] It is, however, more complex mainly

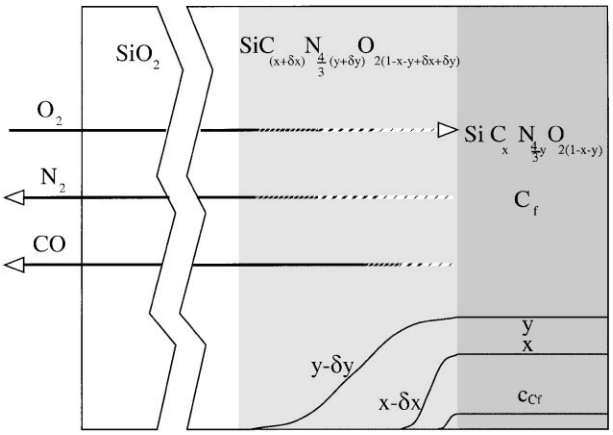

Fig. 8. Tentative schematic description of the oxidation of Si–C–N–(O) fibres in pure oxygen ($P = 100$ kPa) showing the mass transfer of reactants/products and the concentration profile through the oxide layer and at the oxide/substrate interface.

because of the presence of carbon atoms in the continuum as well as in the free carbon phase. Local analyses by EELS of the oxide/fibre interfacial zone did not support the occurrence of such an intermediate phase, at least at a scale beyond about 10 nm but showed a steep composition gradient between the silica and the Si–C–N–O bulk ceramic.[21–66] However, its presence at a lower scale is not strictly excluded, though not experimentally established.

On the basis of the distinct mechanisms assumed to control the oxidation kinetics of SiC and Si_3N_4, one can suggest that the rate limiting step involved in the oxidation of Si–C–N–O ceramics is the slowest permeation rate of O_2 through either, the SiO_2 layer for low y values (like for instance the Si–C or Si–C–O ceramics) or, if any, the $SiC_{(x-\delta x)}N_{4(y-\delta y)/3}O_{2(1-x-y+\delta x+\delta y)}$ continuum of the sub-layer for high y values (for instance Si_3N_4). In the latter case, the main parameter determining the rate limiting step and the oxidation rate, would be the composition gradient along the thickness of that $SiC_{(x-\delta x)}N_{4(y-\delta y)/3}O_{2(1-x-y+\delta x+\delta y)}$ sub-layer, itself depending on the bulk composition of the Si–C–N–O ceramic and particularly the x and y values. It is worthy of note that the composition change of the continuum along the thickness the sub-layer depends on two parameters [δx and δy in Eq. (18)] instead of only one (δy) for the oxidation of Si_3N_4.[56,57]

For $y = 0$ (Si–C–O ceramics), the experimental results showed that the parameter x has almost no effect on the kinetics. This feature therefore suggests that the permeation of O_2 through the SiO_2 layer, remains the rate limiting step of the oxidation mechanism within the range of x values tested. Furthermore, there is no evidence of the formation of a $SiC_{(x-\delta x)}O_{2(1-x+\delta x)}$ sub-layer for the oxidation of polycrystalline SiC, suggesting in this case, a true SiO_2/SiC interfacial reaction [Eq. (7)].

Conversely, when $y \neq 0$, the parameter y, either alone (for Si–N–O system) or together with x (for Si–C–N–O system), appears to have a determinant influence on the rate limiting step of the oxidation mechanism.

It has been well established for of the oxidation of SiC, that the permeation of O_2 through the SiO_2 scale, as the rate limiting step, is slower than the oxidation reaction itself, i.e., the substitution of Si–O bonds for SiC–bonds at the SiO_2/SiC interface. On the other hand, for the oxidation of Si_3N_4, experimental studies and models account for a simultaneous oxygen diffusion and reaction (the substitution of Si–O for Si–N) through the oxynitride sub-layer. A consequence of that, is that, for a given position within the sub-layer, the diffusion rate of O_2 inwards is of the order of the reaction rate (the substitution of Si–O bonds for Si–N bonds), while both being slower than the O_2 diffusion through the SiO_2 outer scale. Hence, if one extends to the Si–C–N–O ceramics the concept of simultaneous O_2 diffusion/reaction through a depth variable composition sub-layer (but in this case with a two composition parameters δx and δy), a substitution of Si–O for Si–C faster than for Si–N bonds might be expected. It would therefore result in a x profile steeper than the y profile along the depth. The oxidation rate would be therefore controlled by the composition of the oxynitride derived from the partial oxidation of the $SiC_xN_{4y/3}O_{2(1-y)}$ oxycarbonitride, i.e. $SiN_{4y/3}O_{2(1-y)}$ or in other terms as experimentally observed, by the parameter y only (Fig. 8).

5. Conclusion

The oxidation of ceramics from the Si–C–N–O system has been investigated through TGA tests of various commercial and experimental small diameter fibres. The oxidation rates (K_T) and the activation energies (E_a) of the Si–C–O ceramics investigated are close to those for crystalline SiC. Both the oxygen and free carbon concentrations in the ceramic have a limited influence on

the oxidation behaviour. As long as the silica scale formed during oxidation is tight and protective, a parabolic oxidation regime is observed and the oxidation kinetics of the Si–C–O materials are mainly controlled by the diffusion of oxygen through SiO_2. However, because of the thermodynamical instability of the oxygen rich systems, the parabolic regime is no longer observed beyond their intrinsic degradation temperature and the oxidation rate dramatically increases.

The parabolic rates of the nitrogen containing systems (Si–C–N–O and Si–N–O) are generally lower than those for SiC whereas their activation energies are higher. Furthermore, the oxidation kinetics features strongly depend on the fractions of the number of Si–C and Si–N bonds to all Si–i bonds ($i = C, N, O$), i.e. respectively, $x = n_{Si-C}/\Sigma_i n_{Si-i}$ and $y = n_{si-N}/\Sigma_i n_{Si-i}$, with i=C,N,O. The K_T and E_a values continuously vary from those for SiC ($x = 1, y = 0$), typically ranging $E_a = 110 - 140$ kJ mol^{-1}, to those for Si_3N_4 ($x = 0$, $y = 1$), i.e. $E_a = 330-490$ kJ mol^{-1}. The oxidation mechanism in such Si–C–N–O systems might be related to a complex diffusion/reaction regime involving the formation of an intermediate silicon-oxynitride sub-layer (in a similar manner than for Si_3N_4) or even also a silicon-oxycarbonitride layer. Like for the Si–C–O system, the oxidation behaviour in these complex systems is not significantly influenced by the presence of oxygen nor free carbon in the initial ceramics. It might rather be governed by the x and y ratios, limiting the nitrogen concentration gradient of the silicon-oxy(carbo)-nitride sub-layer at the oxide/substrate interface and therefore affecting the diffusion/reaction rates.

Acknowledgements

The author would like to thank Nippon Carbon Co. Ltd. and Ube Industries Ltd. for the supply of the SiC based-fibres. He is indebted to the persons who participated to the preparation and the studies of the experimental fibres and especially D. Mocaer from SNECMA-Le Haillan, K. Berroth and U. Vogt from the EMPA-Duebendorf. He also gratefully thanks R. Naslain and R. Pailler from LCTS and R.E. Tressler and K. Spear from the Dept. of Mater. Sci. and Eng.-Pennsylvania State University, for valuable discussions.

References

1. Chermant, J. L., *Les Céramiques Thermomécaniques*. Presses du CNRS, Paris, 1989.
2. Washburn, M. E., Silicon oxynitride refractories. *Am. Ceram. Soc. Bull*, 1967, **46**(7), 667–671.
3. Hasegawa, Y., Iimura, M. and Yajima, S., Synthesis of continuous silicon fibers, part 2: conversion of polycarbosilane fibre into silicon carbide fibers. *J. Mat. Sci.*, 1980, **15**, 720–728.
4. Yamamura, T., Ishikawa, T., Shibuya, M. and Okamura, K., Development of a new continuous silicon-titanium-carbon-oxygen fiber using an organometallic polymer precursor. *J. Mat. Sci.*, 1988, **23**, 2589–2594.
5. Okamura, K., Matsukawa, T. and Hasegawa, Y., γ-Ray irradiation curing on polycarbosilane fibers as the precursor of SiC fibers. *Mat. Sci. Letters*, 1985, **4**, 55–57.
6. Okamura, K., Sato, M., Segushi, T. and Kawanishi, S., Preparation of high-temperature strength SiC fiber in controlled interphases. In *Composite Materials*, ed. H. Ishida. Elsevier Science Publishing, Amsterdam, 1990, pp. 209–218.
7. Deleeuw, D. C, Lipowitz, J. Preparation of substantially crystalline silicon carbide fibers from polycarbosilane. Eur. Pat. No. 0 438 117 A1, 15 January 1991.
8. Lipowitz, J., Barnard, T., Bujalski, D., Rabe, J. A., Zank, G. A., Zangvil, A. and Xu, Y., Fine-diameter polycrystalline SiC fibers. *Comp. Sci. Tech.*, 1994, **51**, 167–171.
9. Toreki, W., Batich, C. D., Sacks, M. D., Saleem, M., Choi, G. J. and Moronne, A. A., Polymer-derived silicon carbide fibers with low-oxygen content and improved thermomechanical stability. *Comp. Sci. Tech.*, 1994, **51**, 145–159.
10. Hasegawa, Y., New curing method for polycarbosilane with unsaturated hydrocarbons and application to thermally stable SiC fiber. *Comp. Sci. Tech.*, 1994, **51**, 161–166.
11. Chollon, G., Czerniak, M., Pailler, R., Bourrat, X., Pillot, J. P., Naslain, R. and Cannet, R., A model SiC-based fibre with a low oxygen content prepared from a polycarbosilane precursor. *J. Mat. Sci.*, 1997, **32**, 893–911.
12. Yamamura, T., Tyranno fibers, EACM, ECCM-6, Euro-Japanese Colloquium on Ceramic Fibers, Japan Soc. Comp. Mat., ed. A.R. Bunsell and I. Kimpara, Bordeaux, 23–24 Sept. 1993.
13. Okamura, K., Sato, M. and Hasegawa, Y., Silicon nitride fibers and silicon oxynitride fibers obtained by the nitridation of polycarbosilane. *Ceramics International*, 1987, **13**, 55–61.
14. Mocaer, D., Pailler, R., Naslain, R., Richard, C., Pillot, J. P., Dunogués, J., Delverdier, O. and Monthioux, M., Si–C–N ceramics with a high microstructural stability elaborated from the pyrolysis of new polycarbosilazane precursors, part III: effect of pyrolysis conditions on the nature and properties of oxygen-cured derived monofilaments. *J. Mat. Sci.*, 1993, **28**, 2639–2653.
15. Mocaer, D., Pailler, R., Naslain, R., Richard, C., Pillot, J. P., Dunoguès, Darnez, J. C., Chambon, M. and Lahaye, M., Si–C–N ceramics with a high microstructural stability elaborated from the pyrolysis of new polycarbosilazane precursors, part IV: oxygen-free monofilaments. *J. Mat. Sci.*, 1993, **28**, 3049–3058.
16. Pailler, R., Chollon, G., Hannache, H., Naslain, R., Pillot, J. P., Dunogués, J. and Birot, M., Influence of different curing processes on the thermal stability of ceramic fibers derived from organosilicon precursors, Adv. Stuct. Fiber Comp. In *Advances in Science and Technology*, ed. P. Vincenzini ed. Techna Publishers, Faenza, 1995, pp. 69–76.
17. Funayama, O., Nakahara, H., Tetsuka, A., Ishii, T. and Isoda, T., Development of Si–B–O–N fibres from polyborsilazane, J. *Mat. Sci.*, 1994, **29**, 2238–3344.
18. Milewski, J. V., Gac, F. D., Petrovic, J. J. and Skaggs, S. R., Growth of beta-silicon carbide whiskers by VLS process. *J. Mat. Sci.*, 1985, **20**(4), 1160–1166.
19. Wang, M. J. and Wada, H., Synthesis and characterization of silicon nitride whiskers. *J. Mat. Sci.*, 1990, **25**, 1690–1698.
20. Cunningham, A. L. and Davies, L. G., Preparation and characterization of a novel form of Si_3N_4 fibres. Proc. 15th SAMPE, 1969, pp. 209–217
21. Chollon, G., Vogt, U. and Berroth, K., Processing and characterization of an amorphous Si–N–O fibre. *J. Mat. Sci.*, 1998, **33**, 61529-1540.
22. Laffon, C., Flanck, A. M., Lagarde, P., Laridjani, M., Hagege, R., Olry, P., Cotteret, J., Dixmier, J., Miquel, J. L., Hammel, H. and Legrand, A. P., Study of Nicalon-based ceramic fibres and

powders by EXAFS spectrometry, X-ray diffractometry and some additional methods. *J. Mat. Sci.*, 1989, **24**, 1503–1512.
23. Porte, L. and Sartre, A., Evidence for a silicon oxycarbide phase in the nicalon silicon carbide fibre. *J. Mat. Sci.*, 1989, **24**, 271–275.
24. Le Coustumer, P., Monthioux, M. and Oberlin, A., Understanding nicalon fiber. *J. Eur. Ceram. Soc.*, 1993, **11**, 95–103.
25. Lipowitz, J., Freeman, H. A., Chen, R. T. and Prack, E. R., Composition and structure of ceramic fibers prepared from polymeric precursors. *Adv. Ceram. Mater.*, 1987, **2**, 2121-128.
26. Chaim, R. and Heuer, A. H., Microstructural and microchemical characterization of silicon carbide and silicon carbonitride ceramic fibers produced from polymer precursors. *J. Am. Ceram. Soc.*, 1988, **71**(1), 960–969.
27. Mah, T., Lecht, N., McCullum, D. E., Hoenigman, J. R., Kim, H. M., Katz, A. P. and Lipsitt, H. A., Thermal stability of SiC fibers nicalon. *J. Mat. Sci.*, 1984, **19**, 1191–1201.
28. Johnson, S. M., Brittain, R. D., Lamoreaux, R. H. and Rowcliffe, D. J., Degradation mechanisms of silicon carbide fibers. *J. Am. Ceram. Soc.*, 1988, **71**, C132–C135.
29. Clark, T. J., Jaffe, M., Rabe, J. and Langley, N. R., Thermal stability characterization of SiC ceramic fibers: I mechanical property and chemical structure effects. *Ceramic Engineering and Science Proceedings*, 1986, **7**(7–8), 901–913.
30. Bender, B. A., Wallace, J. S. and Schrodt, D. J., Effects of thermochemical treatments on the strength and microstructure of SiC fibers. *J. Mat. Sci.*, 1991, **26**, 970–971.
31. Bodet, R., Jia, N. and Tressler, R. E., Microstructural instability and the resultant strength of Si–C–O nicalon and Si–N–C–O HPZ fibres. *J. Eur. Ceram. Soc.*, 1996, **16**, 653–664.
32. Takeda, M., Imai, Y., Ichikawa, H., Ishikawa, T., Kasai, N., Segushi, T. and Okamura, K., Thermal stability of the low oxygen silicon carbide fibers derived from polycarbosilane. *Ceram. Eng. Sci. Proc*, 1992, **13**(7–8), 209–217.
33. Chollon, G., Pailler, R., Naslain, R., Laanani, F., Monthioux, M. and Olry, P., Thermal stability of a PCS-derived SiC fiber with a low oxygen content Hi-nicalon. *Mat. Sci.*, 1997, **32**, 327–347.
34. Chollon, G., Aldacourrou, B., Capes, L., Pailler, R. and Naslain, R., Thermal behaviour of a polytitanocarbosilane-derived fibre with a low oxygen content: the tyranno lox-E fibre. *J. Mat. Sci.*, 1998, **33**, 901–911.
35. Matsuo, H., Funayama, O., Kato, T., Koya, H. and Isoda, T., Crystallisation behavior of high purity amorphous silicon nitride fibers. *J. Ceram. Soc. Japan*, 1994, **102**(5), 409–413.
36. Costello, J. A. and Tressler, R. E., Isotope labeling studies of the oxidation of silicon at °C and 1300°C. *J. Electrochem. Soc.*, 1984, **1000**, 131(8), 1944-1947.
37. Harris, R. C. A., Oxidation of 6H-α silicon carbide platelets. *J. Am. Ceram. Soc.*, 1975, **58**(1–2), 7–9.
38. Costello, J. A. and Tressler, Oxidation kinetics of silicon carbide crystals and ceramics: I, in dry oxygen. *J. Am. Ceram. Soc.*, 1986, **69**(9), 674–681.
39. Zheng, Z., Tressler, R. E. and Spear, K. E., Oxidation of single-crystal silicon carbide. Part I. experimental studies. *J. Electrochem. Soc.*, 1990, **137**(3), 854–858.
40. Zheng, Z., Tressler, R. E. and Spear, K. E., Oxidation of single-crystal silicon carbide. Part II. kinetic model. *J. Electrochem. Soc.*, 1990, **137**(9), 2812–2816.
41. Ramberg, C. E., Spear, K. E., Tressler, R. E. and Chinone, Y., Oxidation behavior of CVD and single crystal SiC at °C. *J. Electrochem. Soc.*, 1995, **1100**, 142(11), L214–L216.
42. Ramberg, C. E., Crutiani, G., Spear, K.E and Tressler, R. E., Passive oxidation kinetics of high purity silicon carbide from 800° to 1100°C. *J. Am. Ceram. Soc.*, 1996, **79**(11), 2897–2911.
43. Zheng, Z., Tressler, R. E. and Spear, K. E., The effects of sodium contamination on the oxidation of single crystal silicon carbide. *J. Electrochem. Soc.*, 1992, **33**(4), 545–556.
44. Zheng, Z., Tressler, R. E. and Spear, K. E., The effects of Cl_2 on the oxidation of single crystal silicon carbide. *J. Electrochem. Soc.*, 1992, **33**(4), 557–567.
45. Ogbuji, L. U. J. T., Effect of oxide devitrification on oxidation kinetics of SiC. *J. Am. Ceram. Soc.*, 1997, **80**(6), 1544–1550.
46. Du, H., Tressler, R. E., Spear, K. E. and Pantano, C. G., Oxidation studies of crystalline CVD silicon nitride. *J. Electrochem. Soc.*, 1989, **136**(5), 1527–1535.
47. Du, H., Tressler, R. E. and Spear, K. E., Thermodynamics of the Si–N–O system and kinetic modelling of oxidation of Si_3N_4. *J. Electrochem. Soc.*, 1989, **136**(11), 3210–3215.
48. Choi, D. J., Fishbach, D. B. and Scott, W. D., Oxidation of chemically-vapor-deposited silicon nitride and single-crystal silicon. *J. Am. Ceram. Soc.*, 1989, **72**(7), 1118–1123.
49. Zheng, Z., Tressler, R. E. and Spear, K. E., A comparison of the oxidation of sodium-implanted CVD Si_3N_4 with the oxidation of sodium implanted SiC-crystals. *J. Corr. Sci.*, 1992, **33**(4), 569–580.
50. Du, H., Houser, C. A., Tressler, R. E., Spear, K..E and Pantano, C. G., Isotopic studies of oxidation of Si_3N_4 and Si using SIMS. *J. Electrochem. Soc.*, 1990, **137**(2), 741–742.
51. Luthra, V., A mixed interface reaction/diffusion control model for oxidation of Si_3N_4. *Electrochem. Soc.*, 1991, **138**(10), 3001–3007.
52. Ogbuji, L. U. J. T. and Smialek, J. L., Evidence from transmission electron microscopy for an oxynitride layer in oxidized Si_3N_4. *J. Electrochem. Soc.*, 1991, **138**(10), .
53. Ogbuji, L. U. J. T., Role of Si_2N_2O in passive oxidation of chemically-vapor-deposited Si_3N_4. *J. Am. Ceram. Soc.*, 1992, **77**(11), 2995–3000.
54. Ogbuji, L. U. J. T., Mechanism of incipient oxidation of bulk chemical vapor deposited Si_3N_4. *J. Electrochem. Soc.*, 1993, **140**(3), 759–766.
55. Ogbuji, L. U. J. T. and Bryan, S. R., The SiO_2–Si_3N_4 interface, Part 1: nature of the interphase. *J. Am. Ceram. Soc.*, 1995, **78**(5), 1272–1278.
56. Ogbuji, L. U. J. T. and Bryan, S. R., The SiO_2–Si_3N_4 interface, Part 2: permeation an oxidation reaction. *J. Am. Ceram. Soc.*, 1995, **78**(5), 1279–1284.
57. Sheldon, B. W., Silicon nitride oxidation based on oxynitride interlayers with graded stoichiometry. *J. Am. Ceram. Soc.*, 1996, **79**, 2993–2996.
58. Jacobson, N. S. and Corrosion of silicon-based ceramics in combustion environments, J., Am. *Ceram. Soc.*, 1993, **76**(1), 3–28.
59. Spear, K. E., Tressler, R. E., Zheng, Z. and Du, H. Oxidation of silicon carbide single-crystal and CVD silicon nitride. In *Ceramic Transactions*, ed. R. E. Tressler and M. McNallan. The American Ceramic Society, Westerville Ohio, 1990. vol. **10**, pp. 1–18.
60. Luthra, K. L., Some new perspectives on oxidation of silicon carbide and silicon nitride. *J. Am. Ceram. Soc.*, 1991, **74**(5), 1095–1103.
61. Ogbuji, L. U. J. T. and Opila, E. J., A comparision of the oxidation kinetics of SiC and Si_3N_4. *J. Electrochem. Soc.*, 1995, **142**(3), 925–930.
62. Singhal, S. C., Effect of water vapor on the oxidation of hot-pressed silicon nitride and silicon carbide. *J. Am. Ceram. Soc.*, 1976, **59**(1-2), 81–82.
63. Warren, R. and Anderson, C. H., Silicon carbide fibres and their potential for use in composite materials. Part II. *Composites*, 1984, **15**(2), 101–111.
64. Clark, T. J., Prack, E. R., Haider, M. I. and Sawyer, L. C., Oxidation of SiC ceramic fiber. *Ceramic Engineering and Science Proceedings*, 1987, **8**(7–8), 717–731.
65. Filipuzzi, L. and Naslain, R., Oxidation kinetics of SiC-based ceramic fibers. *Proc. 7th CIMTEC, Mater. Sci. Monograph 68 Adv. Struct. Inorg. Comp.*, ed. P. Vincenzini, Elsevier, Amsterdam, 1991, 35–46

66. Mocaer, D., Chollon, G., Pailler, R., Filipuzzi, L. and Naslain, R., Si–C–N ceramics with a high microstructural stability elaborated from the pyrolysis of new polycarbosilazane precursors, Part VI: oxidation kinetics of model filaments. *J. Mat. Sci.*, 1993, **28**, 3059–3068.
67. Shimoo, T., Chen, H. and Okamura, K., High-temperature stability of nicalon under Ar or O_2 atmosphere. *J. Mat. Sci.*, 1994, **29**, 456–463.
68. Shimoo, T., Hayatsu, T., Takeda, M., Ichikawa, H., Segushi, T. and Okamura, K., Mechanism of oxidation of low-oxygen SiC fiber prepared by electron radiation curing method. *J. Ceram. Soc. Japan*, 1994, **102**(7), 617–622.
69. Shimoo, T., Kakehi, Y., Kakimoto, K. and Okamura, K., Oxidation kinetics of amorphous Si–Ti–C–O Fibers. *J. Japan Inst. Metals*, 1992, **56**(2), 175–183.
70. Kakimoto, K., Shimoo, T. and Okamura, K., Oxidation-induced microstructural change of Si–Ti–C–O fibers. *J. Am. Ceram. Soc.*, 1998, **81**(2), 409–412.